Computational models of aortic coarctation in hypoplastic left heart syndrome: Considerations on validation of a detailed 3D model

Giovanni Biglino[1], Chiara Corsini[2]*, Silvia Schievano[1], Gabriele Dubini[2], Alessandro Giardini[1], Tain-Yen Hsia[1], Giancarlo Pennati[2], Andrew M. Taylor[1], MOCHA collaborative group[3]*

[1] Centre for Cardiovascular Imaging, UCL Institute of Cardiovascular Science, and Great Ormond Street Hospital for Children, NHS Foundation Trust, London - UK

[2] Laboratory of Biological Structure Mechanics, Chemistry, Materials and Chemical Engineering 'Giulio Natta' Department, Politecnico di Milano, Milano - Italy

[3] Modeling Of Congenital Hearts Alliance (MOCHA) Group (Members are listed in the Appendix)

* These authors contributed equally to this work.

INTRODUCTION

There is increasing recognition of the potential offered by experimental and computational models to address clinical problems and investigate complex hemodynamics in congenital heart disease. Such models can provide output data that can be difficult to acquire *in vivo* because the data can be challenging to measure (e.g., coronary blood flow) or restricted by patient conditions (e.g., immediately post-operative). Compared to *in vivo* analyses, both experimental and computational modeling methodologies have the advantage of creating reproducible and controllable environments in which data can be systematically acquired and parametric studies performed (1-3). *In vitro* models are valuable for device fatigue testing (4), and as teaching and practice tools (5), allowing for device implantation and physical manipulations, naturally taking into account fluid-structure interaction phenomena. On the other hand, *in silico* models can provide full fields of local fluid dynamics quantities, such as wall shear stress (6, 7), and the boundary conditions and model parameters can be conveniently set as constant (8, 9). Importantly, once a computational model has been shown to behave accurately, new cases (involving new patients or new devices) can be easily implemented without the time burden associated with dismantling and re-mounting an experimental rig, offering a great degree of flexibility. However, it is crucial to demonstrate the reliability of the computational model by means of a suitable validation study.

Validation is a process whereby results from the computational method are verified against those physically observed (10-13); *in vitro* measurements can be a valuable source of validation data for this process. Once the model is thoroughly validated, the study can be taken forward *in silico* with confidence. Additionally, a synergy of the two approaches may not only overcome some of the respective limitations, but also provide complimentary understanding of the processes involved.

One physiologically challenging scenario to which this modeling paradigm can be beneficially applied is palliated hypoplastic left heart syndrome (HLHS). Newborns with HLHS follow a complex, staged surgical pathway (14), and may present additional complications such as aortic coarctation (15, 16). First-stage palliation of HLHS, that is, the Norwood procedure (17), and aortic coarctation have been studied both experimentally and computationally (18, 19), using either idealized (20, 21) or patient-specific models (1, 7, 8, 22), including multi-scale – also known as multi-domain (23) – studies (8, 22, 24). The Norwood procedure (or stage 1 surgery) is performed just a few days after birth, as HLHS can now be diagnosed *in utero* (25). It aims to provide a source of pulmonary blood flow following the natural closure of the ductus arteriosus, while also improving systemic blood flow through the otherwise hypoplastic ascending aorta. The aorta is typically enlarged during surgery by means of a patch while pulmonary blood flow is sourced via a shunt. Three main shunt types can be used during stage 1, depending on the surgeon's expertise and center preference: a) modified Blalock-Taussig from the innominate artery to the right pulmonary artery (26); b) conduit from the right ventricle to the pulmonary artery or Sano shunt (27); c) central shunt from the ascending aorta to the pulmonary artery (28).

The usefulness of a modeling approach in this context is multifaceted. For instance, different virtual procedures can be performed on a case-by-case basis to provide patient-specific data regarding which approach would be the most beneficial, also highlighting potential hemodynamic differences inherent to different surgical strategies (18, 29). Also, less invasive approaches can be simulated, as in the case of computational models of the hybrid Norwood procedure (20, 30). Focusing on coarctation, cases have been reported in which a non-invasive measurement alone is unable to diagnose the severity of the narrowing, due to significant disagreement between a catheter gradient and a Doppler-derived gradient. For example, the former may be very mild or null while the latter reports >50 mmHg for the same patient (31). Additional hemodynamic insight in such cases could be precious and could be gained by using an appropriate engineering model.

However, a validated Norwood model is currently lacking. Hence, this study aims to construct a multi-scale model of Stage 1 circulation, including aortic coarctation, and to validate it against *in vitro* data.

MATERIALS AND METHODS

Patient selection

A patient with HLHS (3 months old, male) was selected. The patient was diagnosed with aortic and mitral atresia and the ascending aorta was hypoplastic. A Norwood procedure was performed. At 3 months following this operation, exam-

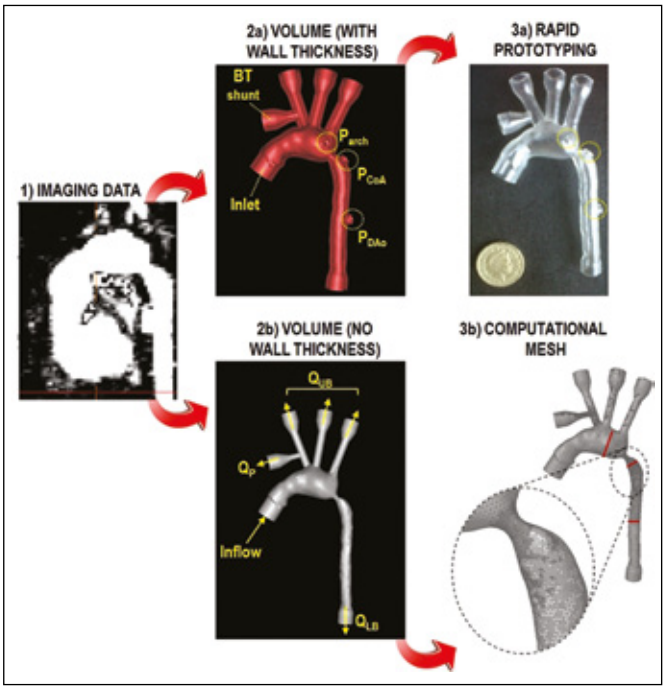

Fig. 1 - *Patient-specific aortic model: magnetic resonance imaging data, showing the coarctation of the aorta **(1)**; 3D volume reconstructed from the imaging data, with added arbitrary wall thickness **(2a)**, for rapid prototyping; rapid prototyped model for in vitro measurements **(3a)**; same 3D model for computational simulations **(2b)** and mesh **(3b)** showing, in red, the cross-sections for pressure calculations (corresponding to the pressure ports highlighted in yellow in **2a** and **3a)**. The coarctation region is zoomed in **3b**, to show the finer meshing.*

ination with magnetic resonance (MR) imaging (1.5 T Avanto scanner; Siemens AG, Erlangen, Germany) and catheterization was performed. The patient had aortic coarctation with a coarctation index of 0.5; the index is defined as the ratio of the isthmus diameter and the diameter of the descending aorta (32). The local Research Ethics Committee approved the use of imaging data for research purposes. The parents gave informed consent for use of the data.

Anatomical model

A patient-specific anatomical model of the aortic arch was created from the available MR data (Fig. 1-1) using commercial software (Mimics®; Materialise NV, Leuven, Belgium) (24, 33). The whole heart sequence was used to reconstruct the patient's anatomy. The images were obtained in a sagittal orientation by using a magnetization-prepared, three-dimensional (3D) balanced, steady-state, free precession sequence (slice thickness = 1 mm, TR = 258.9, TE = 1.8, flip angle = 90°, acquisition matrix = 256 x 152, voxel size = 0.5 x 0.5 x 0.5 mm, pixel bandwith = 590 Hz). Once a 3D volume was obtained and suitably modified for connection and measurements in a mock circuit (Fig. 1-2a), the model was rapid prototyped (Fig. 1-3a) using a robust transparent resin (Watershed® 11122; DSM Somos, Elgin, IL, USA) with an arbitrary uniform wall thickness of 1.5 mm to guarantee the model's robustness. The printer used for printing the model (Viper si2 SLA System 3D Printer, 3D Systems Corp., Rock Hill, SC, USA) has a resolution of 16 µm, in accordance with PolyJet technology (34). The accuracy of printing in relation to the resolution of the image-derived 3D models has been discussed in a separate publication (33).

The model has one inlet (ascending aorta), five outlets (three brachiocephalic vessels, descending aorta and modified Blalock-Taussig, mBT, shunt) and three ports (highlighted in yellow in Fig. 1-2a and 3a) on the aortic wall to allow for pressure measurements at the following locations: a) arch (P_{arch}); b) just after the coarctation (P_{CoA}); c) about 10 isthmus diameters downstream from the coarctation, accounting for pressure recovery (P_{DAo}). The inlet of the model had an internal diameter of 9 mm, the isthmus diameter was 2.7 mm, and the diameter of the descending aorta was 5.7 mm. The pressure ports were sized for a 5 F catheter.

Experimental study

The phantom was inserted into a mock circulatory system (Fig. 2), described in detail in a separate publication (24). The system was filled with a solution of 33.5% glycerine in water by weight, accepted in the literature as a suitable blood analogue (24). Three lumped impedances (resistive R and compliant C elements) were used as downstream boundary conditions for the upper body (UB, merging the brachiocephalic outlets), lower body (LB, connected to the descending aorta) and pulmonary circulation (P, connected to the mBT shunt equivalent conduit). The C elements were Windkessel chambers of adjustable air volume, implementing C of 0.10, 0.57, and 0.54 ml $mmHg^{-1}$, for UB, LB, and P, respectively. The R elements were metered, needle-pinch valves. Two different valve closure settings were adopted to implement appropriate resistances for the systemic and pulmonary vascular beds. Preliminary measurements at different steady flow rates clearly indicated a non-linear behavior (Fig. 3) that can be expressed as $\Delta P_i \approx \alpha_i Q_i^2 + \beta_i Q_i$, with i = UB, LB or P,

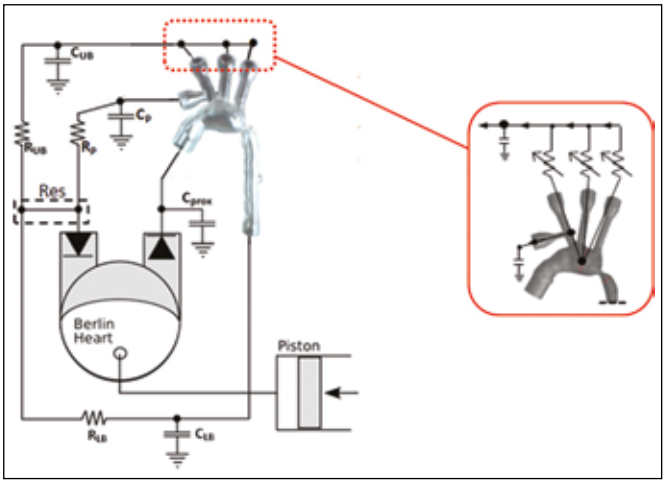

Fig. 2 - *3D aortic model inserted in the mock circulatory system. Each lumped outlet (UB = upper body, LB = lower body, P = pulmonary) is represented by a compliance (C) and a resistance (R) connected to a reservoir (Res) providing constant head pressure and feeding back to the Berlin Heart. A proximal compliance chamber (Cprox) simulates aortic arch compliance. In the* ***red box:*** *detail of the arrangement of non-linear R describing the physical connection between UB outlets by means of a manifold.*

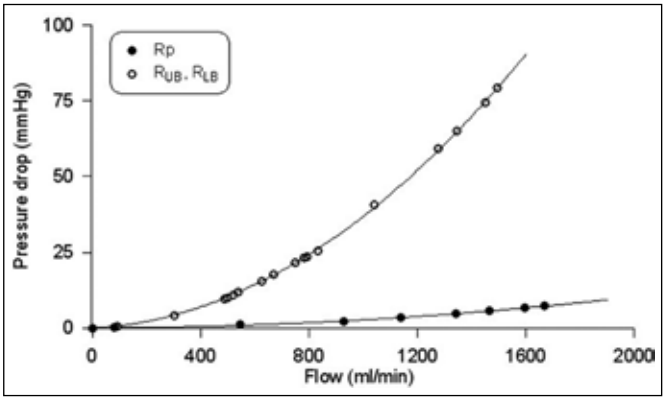

Fig. 3 - *Pressure drop - flow curves ($\Delta P \approx \alpha Q^2 + \beta Q$) characterizing the needle-pinch valves that implement resistances in the mock circuit. The curve with open circles (α = 32.7 mmHg min^2 l^{-2}, β = 4.17 mmHg min l^{-1}) represents R_{UB} and R_{LB}; the curve with full circles (α = 2.46 mmHg min^2 l^{-2}, β = 0.236 mmHg min l^{-1}) represents R_P.*

ΔP_i = pressure drop and Q_i = flow across the component *i*. Coefficient values were: $\alpha_{UB} = \alpha_{LB}$ = 32.7 mmHg min^2 l^{-2}, α_P = 2.46 mmHg min^2 l^{-2}, $\beta_{UB} = \beta_{LB}$ = 4.17 mmHg min l^{-1} and β_P = 0.236 mmHg min l^{-1}. The outlets were connected to a reservoir open to the atmosphere, providing a constant pressure of 16 mmHg and feeding back to the ventricle. Hydrodynamic data were acquired during pulsatile flow. Pressure was measured using a factory-precalibrated, fiber-optic sensor (Preclin 420; Samba Sensors, Västra Frölunda, Sweden) inserted via the three pressure ports on the 3D model. Flow was measured with ultrasonic flow probes (9PXL; Transonic, Ithaca, NY, USA) snugly fitted at each outlet. Data were recorded at 250 Hz (AcqKnowledge; Biopac Systems, Goleta, CA, USA). The settings (heart rate HR = 125 bpm, stroke volume = 16.3 mL and diastolic time fraction = 50%) were representative for a Norwood patient (2).

Fluid temperature was monitored during the experiments (22.8 ± 0.2°C). Viscosity was not directly measured, and this uncertainty was accounted for in the computational study. The water-glycerine solution used *in vitro* was assumed as an incompressible Newtonian fluid with density (ρ) of 1060 kg m^{-3} and viscosity (μ) of 3.6 cP (24).

Computational study

The same geometry used for the rapid prototyping process represented the 3D rigid-walled element of the *in silico* multi-scale system (Fig. 1-2b). The anatomical model included elements strictly related to the *in vitro* tests, such as the fanning outlets that were specifically designed for connecting the model into the mock circuit in order to ensure the goodness of the match. The only difference was the absence of the pressure ports. Pressure was instead monitored at three cross-sections (Fig. 1-3b in red), corresponding to the same locations as the pressure ports. The 3D model was meshed with an unstructured grid (Fig. 1-3b) of around 380 000 tetrahedral elements with a global maximum edge size of 0.001 m, in particular not exceeding 2e-4 m at the coarctation site, and 4e-4 m at the shunt anastomosis (Gambit 2.3.16- Fluent, ANSYS, Canonsburg, PA, USA). This mesh was chosen after carrying out a sensitivity analysis: the grid was progressively adapted according to pressure and velocity gradients (based on preliminary simulation results), approximately doubling the number of elements and ensuring that the pressure drops across the model did not change more than 2%. This procedure enabled the final number of elements to be limited by using a refined grid only in proximity of the most critical hemodynamic regions, i.e. the aortic coarctation (Fig. 1-3b, zoom) and the shunt anastomosis.

The lumped parameter network (LPN) attached to the 3D geometry, including non-linear R and constant C elements, was set according to the *in vitro* model, with a downstream pressure of 16 mmHg. On top of these impedances, a non-linear resistance was added upstream of the UB compliance,

to account for a manifold merging the brachiocephalic outlets in the *in vitro* setting. Based on the manifold geometry and on the hydraulics formula (35) for multiple perpendicular connections, the pressure drops across the manifold ($\Delta P_m = k_m Q_{UB}^2$) were estimated using a constant parameter k_m = 30 mmHg min^2 l^{-2}. The parameter was split in three non-linear resistances, equal to 90 mmHg min^2 l^{-2}, attached to the UB outlets and merged upstream C_{UB} (Fig. 2, red box). In other words, a parallel of the UB branches equivalent to k_m was hypothesized, considering ($P_{arch} - P_{UB}$) as representative of manifold dissipations.

The inflow boundary condition was assigned as the Fourier series of the velocity waveform derived from the sum of the three outflows (Q_{UB}, Q_{LB} and Q_P) measured *in vitro* (Fig. 5, left) since measurement of a Q signal at the inlet of the experimental aortic model was not feasible.

Flow regime and multi-scale simulations

Starting from the multi-scale model described above, a number of pulsatile simulations were carried out using commercial software (Fluent 12.1.4; ANSYS, Canonsburg, PA, USA). A multi-scale coupling approach (36) was adopted imposing time-varying uniform pressures, calculated by the LPN, at each outlet of the 3D domain. Time-varying flow rates averaged over the boundary sections were the forcing terms of the LPN. The LPN description resulted in a non-linear algebraic-differential equations system with a variable number of equations, according to the simulation features. The implicit Euler method was used as the time integration technique for solving Navier-Stokes equations in the 3D domain, while the explicit Euler method was used for solving the LPN system. The time step was fixed at 5·10^{-5} s and four consecutive cycles were considered sufficient to reach a stable solution. The average time to complete one cardiac cycle was ~ 20 h, using an Intel® Core™ i7 (3 GHz) personal computer.

A complex hemodynamic arrangement like the Norwood circulation with coarctation may develop turbulence, and some phenomena occurring *in vitro* may not be captured depending on the *in silico* flow regime assumption. According to the peak flow rates (Q_{pk}) measured *in vitro* (i.e. Q_{pk} through the coarctation = 0.85 L min^{-1} and Q_{pk} through the shunt = 1.17 L min^{-1}), the vessel sizes D (coarctation diameter = 2.7 mm and shunt diameter = 2.6 mm), and HR = 125 bpm, peak Reynolds number ($Re = 4*\rho*Q_{pk}*(\pi*D*\mu)^{-1}$) and Womersley number ($Wo = D*(\rho*\pi*HR*(2*\mu)^{-1})^{0.5}$) were 1 967 and 2.6 in the coarctation, and 2 812 and 2.5 in the proximal shunt, respectively.

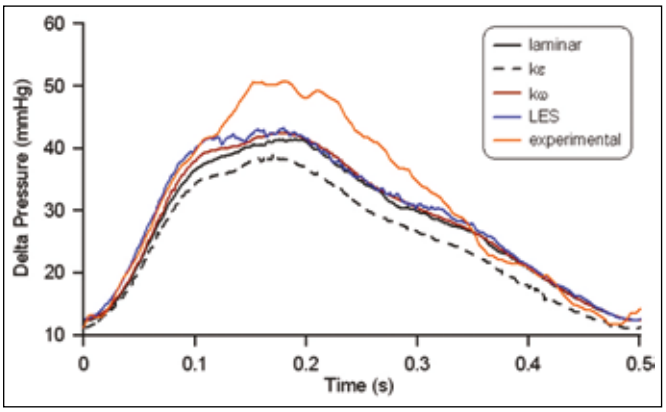

Fig. 4 - *Pressure drop (P_{arch}-P_{DAo}) across the coarctation resulting from simulations A1* ***(black),*** *A2* ***(dashed black)****, A3* ***(red)****, and A4* ***(blue),*** *compared with the in vitro measured signal* ***(orange)****.*

The stand-alone 3D model was first used for a set of simulations (A1-A4) to define the best flow regime description, which was then verified in a multi-scale arrangement (A5).

- Simulation A1: laminar flow;
- Simulation A2: *k*-ε turbulence model, as suggested by Qian et al (7); turbulent kinetic energy = 1 m^2/s^2, turbulent dissipation rate = 1 m^2/s^3;
- Simulation A3: *k*-ω *SST* turbulence model as suggested by Varghese et al (37); turbulent kinetic energy = 1 m^2/s^2, specific dissipation rate = 1 s^{-1};
- Simulation A4: *LES* turbulence model using a finer mesh (650 000 elements), as suggested by Varghese et al (37), and the "No perturbations" fluctuating velocity algorithm

In simulations A1-A4 the experimental flow tracings were imposed at the UB and P model outlets, while a reference pressure was set at the LB outlet. The best flow regime model was assessed by comparing all the pressure drops obtained across the coarctation (P_{arch} - P_{DAo}) with the measured data. Having opted for the most appropriate flow regime, the multi-scale simulation (A5) was performed for comparison with *in vitro* data.

The effect of possible changes of fluid properties was also investigated. The viscosity of aqueous-glycerine solutions is highly sensitive to temperature variations and glycerine content (38), and a rigorous control of viscosity during different *in vitro* test sessions cannot be guaranteed. Hence, an additional multi-scale simulation (B5) was performed imposing lower fluid viscosity (=2.7 cP).

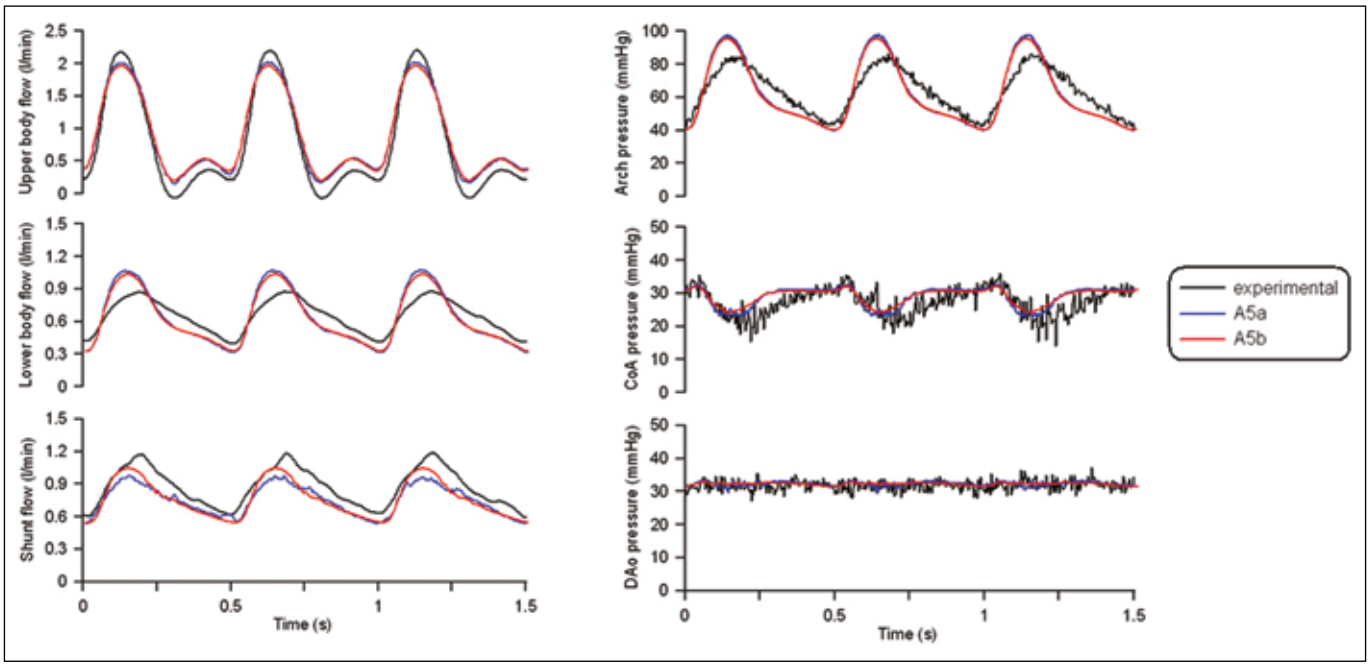

Fig. 5 - *Comparison of multi-scale simulation results **(A5a** and **A5b)** with in vitro data, showing flow tracings at the three outlets (on the left) and pressure signals measured at three locations along the aorta (on the right).*

RESULTS

Figure 4 reports the comparison of the A1-A4 results with the experimental data in terms of pressure drop across the coarctation (P_{arch} - P_{DAo}). Results indicated that all the numerical models underestimated the actual pressure drop, particularly at peak systole. Overall, flow regime models produced very similar findings (mean error of ~12%), except for the *k*-ε model, which was less accurate (18% mean error). More specifically, the LES approach yielded a slightly more accurate agreement than traditional turbulence models (11% mean error), but at the expense of a greater computational cost (37), approximately 6 times longer. Since *k*-ω and laminar flow regime models were comparable both in terms of results and computational expense, it was ultimately decided to test both of them in a multi-scale fashion by repeating simulation A5 twice (indicated as simulations A5a and A5b for laminar and *k*-ω models, respectively).

Overall, predicted flows resulting from both simulations A5a and A5b presented satisfactory agreement with the experimental data (Fig. 5). *In vitro* flow signals were all well reproduced, both qualitatively in terms of time tracings as well as quantitatively in terms of their mean values. Flow distribution as % inlet flow was in good agreement

TABLE I - COMPARISON BETWEEN MULTI-SCALE SIMULATION (A5a) AND *IN VITRO* RESULTS

Model	Flows (% Q_{in})			Pressures (mmHg)		
	Q_{UB}	Q_{LB}	Q_P	P_{arch}	P_{CoA}	P_{DAo}
In silico	39.0	28.0	33.0	62.3	28.9	32.3
In vitro	34.0	28.4	37.6	65.1	27.8	31.6

Values of flow distribution (as % inlet flow Qin) at the upper body (UB), lower body (LB), and pulmonary (P) outlets, and values of mean aortic pressure at the three measurement sites (arch, coarctation, CoA, and descending aorta, DAo).

(Tab. I). Q_{LB} was in excellent agreement (28.0% *in silico* vs. 28.4% *in vitro*, 1.4% difference), albeit qualitatively the computed tracing presented slightly more accentuated pulsatility. However, Q_P was somewhat underestimated *in silico* (33.0% vs. 37.6%) to the advantage of the UB outlet. Mean pressure was also in satisfactory agreement at all three measurement locations (Tab. I), with a maximum difference of 4% in the aotic arch (65.1 vs. 62.3 mmHg) and a difference as low as 1% at the coractation port (27.8 vs. 28.9 mmHg). Qualitatively, the oscillations in the aortic arch and the lack of pulsatility in the descending aorta were both captured, although pressure pulse in the aortic arch was accentuated *in silico* (still with

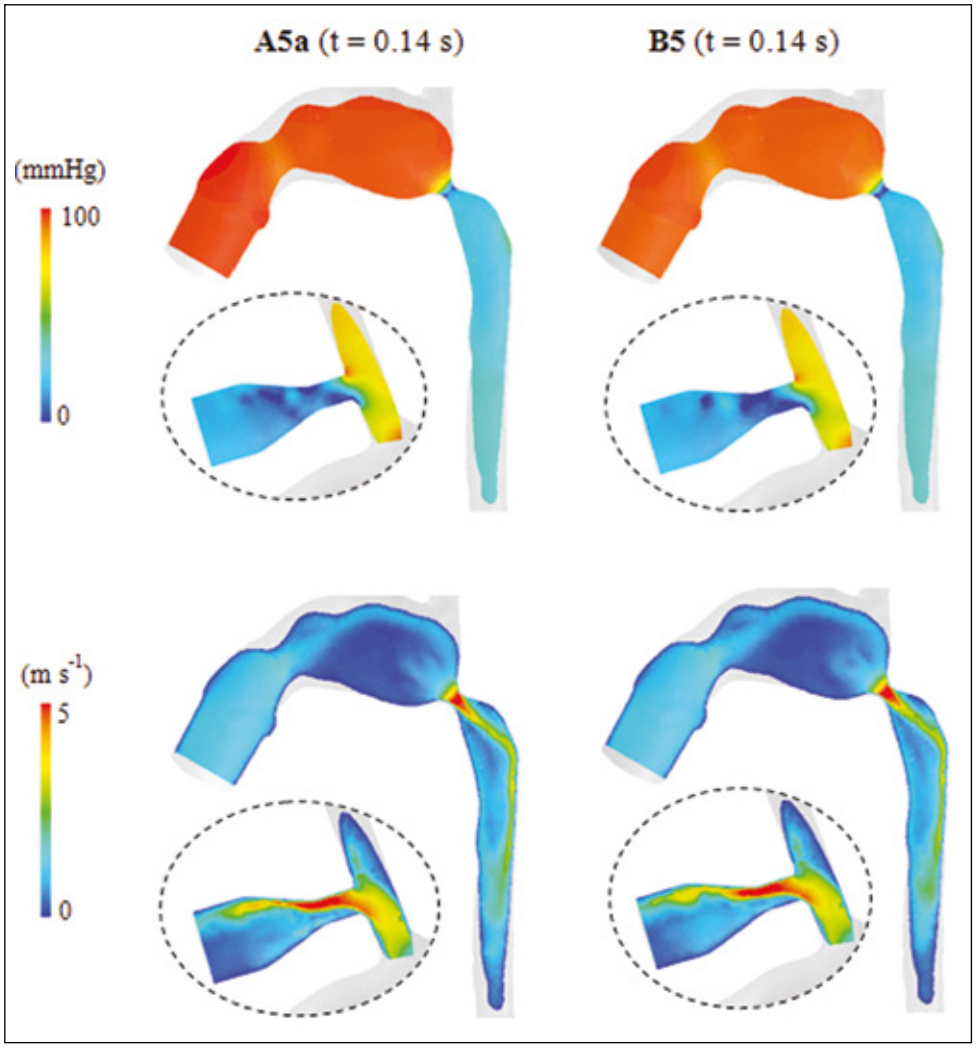

Fig. 6 - *Comparison of multi-scale simulations with higher (3.6 cP) and lower (2.7 cP) viscosity (***A5a** *and* **B5***, respectively), showing the nearly negligible effect of such change on both pressure (top) and velocity (bottom) maps.*

close agreement of the mean values). The A5a and A5b simulations confirmed good performance of both flow regimes in reproducing experimental data, with comparable computational costs. Since a laminar flow model requires fewer assumptions about numerical parameters than a turbulence model (because in a *k*-ω model two additional differential equations need to be solved besides the Navier-Stokes equations), simulation B5 was performed using a laminar flow regime.

Figure 6 shows pressure and velocity maps obtained with simulation B5 compared with the A5a results, highlighting the fact that a substantial variation in fluid viscosity does not affect the hemodynamics in this specific scenario. Pressure and flow tracings for this comparison are shown in Figure 7.

DISCUSSION

This study presents a multi-domain model of the circulation following Stage 1 palliation of HLHS. The same anatomical model, reconstructed from MR data, was used as the 3D element for both *in vitro* and *in silico* simulations. The comparison of the two models allowed validation of the *in silico* approach and definition of the appropriate flow regime assumption for additional computer simulations.

In order for the multi-domain model to achieve good performance values, it had to include not only the 3D model and LPN used *in vitro*, but also a resistive component accounting for additional pressure drops produced by the UB manifold. Based on the A1-A4 results, both the laminar and turbulent *k*-ω flow assumptions were applied to the same

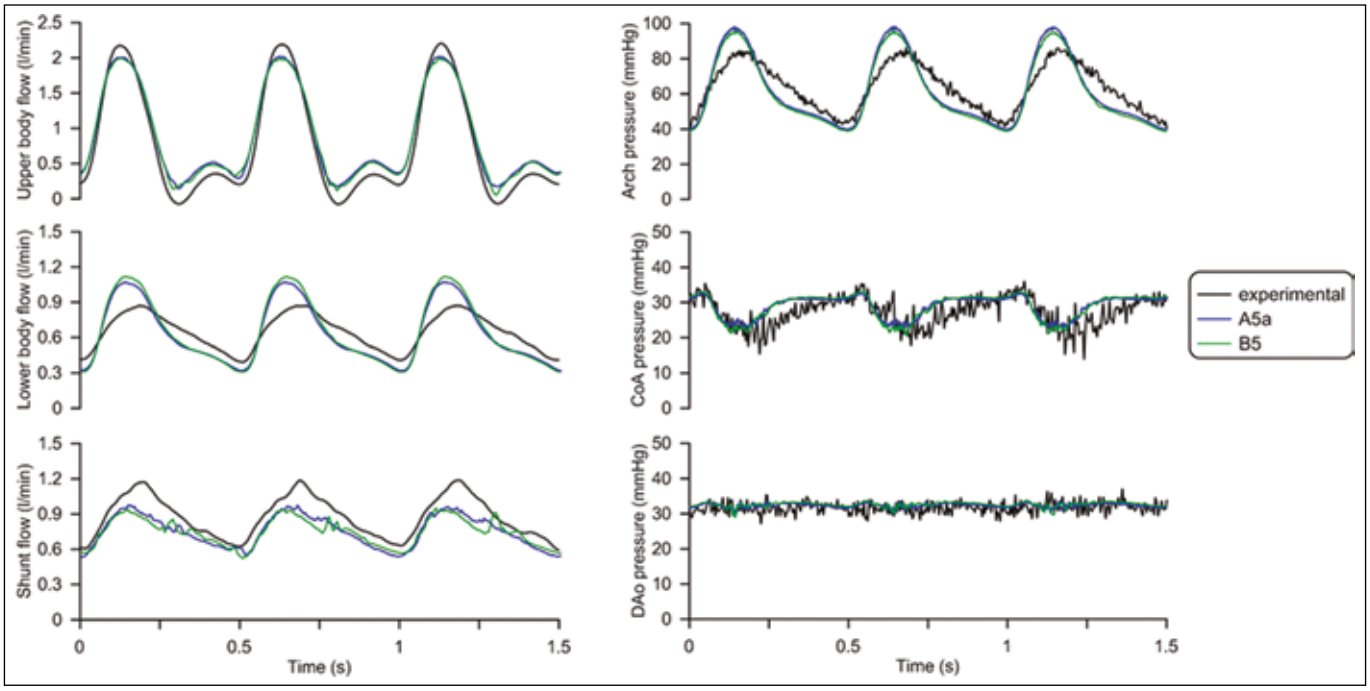

Fig. 7 - *Comparison of multi-scale simulations with higher (3.6 cP) and lower (2.7 cP) viscosity* ***(A5a*** *and* ***B5****, respectively) with in vitro data, showing flow tracings at the three outlets (on the left) and pressure signals measured at three locations along the aorta (on the right).*

multi-scale model (simulations A5a and A5b), set according to experimental data. An overall satisfactory agreement was achieved with respect to the *in vitro* model in terms of the time tracings and the mean values from both the A5a and A5b simulations. This suggests that, although the shunt and the coarctation were characterized by transition to turbulence, this fluid dynamic condition did not influence the flow regime in the other regions of the 3D model. Therefore, simulation B5, investigating the effect of varying viscosity, was performed using a laminar assumption. A possible solution to avoid the choice of flow regime is the use of direct numerical simulations, so that no assumptions must be made about the nature of the flow (37). However, this would require the use of finer meshes compared to those used with turbulence models in order to achieve an accurate solution of the fluid dynamic problem, thus increasing the computational cost. Further improvement may be achieved by refining the mesh's region adjacent to the wall, according to the y+ value required by the turbulence model.

The computational multi-scale approach was also applied to evaluate the effect of modifications in fluid viscosity (simulation B5) in order to account for possible uncertainties related to temperature variations during the experiments. The results suggested that even large (25%) variations in viscosity do not significantly influence the hemodynamics of the multi-scale model. Therefore, the difficulty of rigorously controlling the viscosity of the aqueous glycerine solution during different *in vitro* tests would not play a major role in the accuracy of the data. This may be explained by the fact that the main factors responsible for energy dissipation in the investigated anatomy are the aortic coarctation and the shunt. Moreover, needle-pinch valves – additional terms of localized energy dissipations that are thus not very sensitive to viscous effects – were used as the physical components mimicking peripheral vascular R. From a methodological perspective, *in vitro* alternatives that would better replicate the fact that microvasculature resistance is independent of the flow rate are offered by porous media (39) or bundles of small diameter tubes (1). Using these components, fluid viscosity would play a more important role in determining energy losses, however, this kind of lumped resistance is often cumbersome to construct and more difficult to regulate.

Despite the overall agreement, a few incongruities between experimental and computational results remained. These are likely due to the fact that the model disregards the physical presence of mock circuit components such as pipes, which may induce inertial effects to the fluid

motion, and pipe junctions other than the UB manifold, which potentially cause further non-negligible, non-linear energy dissipation. It is also important to assess the clinical relevance of such incongruities. For instance, while Q_{LB} was very accurately reproduced computationally, the distribution between Q_P and Q_{UB} was somewhat unbalanced, with Q_P being underestimated *in silico* (33% of inlet flow vs. 37.6% *in vitro*) to the advantage of Q_{UB}. Looking at the clinically relevant ratio between Q_P and systemic Q ($Q_S = Q_{UB} + Q_{LB}$), these two scenarios result in $Q_P:Q_S = 0.5$ *in vitro* and $Q_P:Q_S = 0.6$ *in silico*. The computational model is thus capturing the same physiological condition ("the same patient") since this difference in $Q_P:Q_S$ is not particularly meaningful clinically. This value of $Q_P:Q_S$, although still within a physiological range reported in the literature (40), is admittedly quite low. This is due to the setting of the *in vitro* model, as discussed elsewhere (24), which represented the real world data that the computational model should have captured, if validated.

The good agreement between experimental and multi-scale computational results allows additional information to be gathered on the local fluid dynamics (pressure maps, velocity maps, wall shear stress maps), which is outputted by the *in silico* model. An example of local fluid dynamics data can be appreciated in Figure 6.

Limitations

This model, including both the experimental phantom and its computational counterpart, does not take into account the distensible nature of blood vessels. This is a limitation of the study. Implementing compliance by means of Windkessel chambers allows for simulating lumped compliance, but using an altogether compliant phantom would be more realistic from a clinical point of view. Compliant models can be manufactured, and materials that are compatible with PolyJet technology and implement suitable distensibility are being investigated (41). If a compliant model was tested *in vitro*, then a fluid structure interaction (FSI) approach would be mandatorily used for the computational simulations.

The model accounts for a patient-specific anatomy of post-Stage 1 palliation single ventricle physiology, including aortic coarctation. However, the model is not set to patient-specific values, as the clinical data were not sufficient to calculate systemic and pulmonary vascular resistances and hence to set the model at a patient-specific level. The *in vitro* model is, nevertheless, representative of a Norwood physiology, with systolic, diastolic, and mean pressure as well as flow distribution comparable to *in vivo* data from the literature (2, 24, 40, 42). This does not impinge on the validation process, whereby the computational model replicates the experimental data.

One limitation of the computational model is that although it did reproduce trends and mean variations in pressure and flow overall, it did not accurately capture peak systolic pressure. This limitation should be improved in the future, as this value is clinically relevant for the assessment of aortic coarctation.

CONCLUSIONS

This study highlights the importance of using experimental data when choosing the appropriate mesh and flow regime assumptions to preliminarily set up a computational model. A multi-scale model of the circulation following Stage 1 palliation of HLHS, including aortic coarctation, was constructed both *in vitro* and *in silico*, showing satisfactory agreement between the results – provided that the non-linear fluid dynamic phenomena occurring *in vitro* are properly described. This good agreement proved that the computational model is *reliable*. The multi-domain approach was then useful to investigate the hemodynamics in a complex anatomy with several outlets and sources of localized energy dissipations (coarctation and shunt). This approach may next be used to explore the effects of varying coarctation and/or shunt diameter as well as different options for treating coarctation, such as resection, stenting, and ballooning.

APPENDIX 1

Members of MOCHA collaborative group

Andrew Taylor, Alessandro Giardini, Sachin Khambadkone, Silvia Schievano, Marc de Leval, T.-Y. Hsia (Institute of Cardiovascular Sciences, UCL, London - UK); Edward Bove, Adam Dorfman (University of Michigan, Ann Arbor, MI - USA); G. Hamilton Baker, Anthony Hlavacek (Medical University of South Carolina, Charleston, SC - USA); Francesco Migliavacca, Giancarlo Pennati, Gabriele Dubini (Politecnico di Milano, Milan - Italy); Alison Marsden (University of California, San Diego, CA - USA); Jeffrey Feinstein (Stanford University, Stanford, CA - USA); Irene Vignon-Clementel (INRIA, Paris - France); Richard Figliola, John McGregor (Clemson University, Clemson, SC - USA).

Financial Support: The authors gratefully acknowledge the support of the following funding bodies: Fondation Leducq, UK National Institute of Health Research, British Heart Foundation, Royal Academy of Engineering/EPSRC and Heart Research UK. This report is independent research by the National Institute for Health Research Biomedical Research Centre Funding Scheme. The views expressed in this publication are those of the author(s) and not necessarily those of the NHS, the National Institute for Health Research, or the Department of Health.

Conflict of Interest: None.

Address for correspondence:
Dr. Giovanni Biglino
Centre for Cardiovascular Imaging
UCL Institute of Cardiovascular Sciences
& Great Ormond Street Hospital
Great Ormond Street
London WC1N 3JH, UK
g.biglino@ucl.ac.uk

REFERENCES

1. Figliola RS, Giardini A, Conover T, et al. *In vitro* simulation and validation of the circulation with congenital heart defects. Prog Pediatr Cardiol. 2010;30(1-2):71-80.
2. Migliavacca F, Pennati G, Dubini G, et al. Modeling of the Norwood circulation: effects of shunt size, vascular resistances, and heart rate. Am J Physiol Heart Circ Physiol. 2001; 280(5):H2076-H2086.
3. Pennati G, Migliavacca F, Dubini G, Bove EL. Modeling of systemic-to-pulmonary shunts in newborns with a univentricular circulation: State of the art and future directions. Prog Pediatr Cardiol. 2010;30(1):23-29.
4. Lemmon JD. Valve testing: durability and beyond. In: Hijazi ZM, Bonhoeffer P, Feldman T, Ruiz CE, eds. Transcatheter valve repair. Oxon, UK: Taylor & Francis; 2006.
5. Zannoli R, Corazza I, Branzi A. Mechanical simulator of the cardiovascular system. Phys Med. 2009;25(2):94-100.
6. LaDisa JF, Taylor CA, Feinstein JA. Aortic coarctation: recent developments in experimental and computational methods to assess treatments for this simple condition. Prog Pediatr Cardiol. 2010;30(1-2):45-49.
7. Qian Y, Liu JL, Itatani K, Miyaji K, Umezu M. Computational hemodynamic analysis in congenital heart disease: simulation of the Norwood procedure. Ann Biomed Eng. 2010;38(7):2302-2313.
8. Coogan JS, Chan FP, Taylor CA, Feinstein JA. Computational fluid dynamic simulations of aortic coarctation comparing the effects of surgical- and stent-based treatments on aortic compliance and ventricular workload. Catheter Cardiovasc Interv. 2011;77(5):680-691.
9. Migliavacca F, Dubini G, Pennati G, et al. Computational model of the fluid dynamics in systemic-to-pulmonary shunts. J Biomech. 2000;33(5):549-557.
10. Apel J, Neudel F, Reul H. Computational fluid dynamics and experimental validation of a microaxial blood pump. ASAIO J. 2001;47(5):552-558.
11. Babuska I, Oden JT. Verification and validation in computational engineering and science: basic concepts. Comput Methods Appl Mech Eng. 2004;193(36-38):4057-4066.
12. Kung EO, Les AS, Medina F, Wicker RB, McConnell MV, Taylor CA. *In vitro* validation of finite-element model of AAA hemodynamics incorporating realistic outlet boundary conditions. J Biomech Eng. 2011;133(4):041003.
13. Medvitz RB, Kreider JW, Manning KB, Fontaine AA, Deutsch S, Paterson EG. Development and validation of a computational fluid dynamics methodology for simulation of pulsatile left ventricular assist devices. ASAIO J. 2007; 53(2):122-131.
14. Hennein HA, Bove EL. Hypoplastic left heart syndrome. Armonk, NY: Futura Publishing Company; 2002
15. Grech V. Diagnostic and surgical trends, and epidemiology of coarctation of the aorta in a population-based study. Int J Cardiol. 1999;68(2):197-202.
16. Tanous D, Benson LN, Horlick EM. Coarctation of the aorta: evaluation and management. Curr Opin Cardiol. 2009; 24(6):509-515.
17. Norwood WI Jr. Hypoplastic left heart syndrome. Ann Thorac Surg. 1991;52(3):688-695.
18. Kung E, Baretta A, Baker C, et al; Modeling Of Congenital Hearts Alliance (MOCHA)+ Investigators. Predictive modeling of the virtual Hemi-Fontan operation for second stage single ventricle palliation: two patient-specific cases. J Biomech. 2013;46(2):423-429.
19. Oshinski JN, Parks WJ, Markou CP, et al. Improved measurement of pressure gradients in aortic coarctation by magnetic resonance imaging. J Am Coll Cardiol. 1996; 28(7):1818-1826.
20. Corsini C, Cosentino D, Pennati G, Dubini G, Hsia TY, Migliavacca F. Multiscale models of the hybrid palliation for hypoplastic left heart syndrome. J Biomech 2011;44(4): 767-770.
21. Migliavacca F, Balossino R, Pennati G, et al. Multiscale modelling in biofluidynamics: application to reconstructive

paediatric cardiac surgery. J Biomech. 2006;39(6):1010-1020.
22. Olivieri LJ, de Zélicourt DA, Haggerty CM, Ratnayaka K, Cross RR, Yoganathan AP. Hemodynamic Modeling of Surgically Repaired Coarctation of the Aorta. Cardiovasc Eng Technol. 2011;2(4):288-295.
23. Vignon-Clementel IE, Figueroa CA, Jansen KE, Taylor CA. Outflow boundary conditions for three-dimensional finite element modeling of blood flow and pressure in arteries. Comput Methods Appl Mech Eng. 2006;195(29-32):3776-3796.
24. Biglino G, Giardini A, Baker C, et al; MOCHA Collaborative Group. *In vitro* study of the Norwood palliation: a patient-specific mock circulatory system. ASAIO J. 2012;58(1): 25-31.
25. Rychik J. Hypoplastic left heart syndrome: from *in-utero* diagnosis to school age. Semin Fetal Neonatal Med. 2005; 10(6):553-566.
26. Yuan SM, Shinfeld A, Raanani E. The Blalock-Taussig shunt. J Card Surg. 2009;24(2):101-108.
27. Sano S, Ishino K, Kawada M, et al. Right ventricle-pulmonary artery shunt in first-stage palliation of hypoplastic left heart syndrome. J Thorac Cardiovasc Surg. 2003;126(2):504-509, discussion 509-510.
28. Alboliras ET, Chin AJ, Barber G, Helton JG, Pigott JD, Norwood WI. Pulmonary artery configuration after palliative operations for hypoplastic left heart syndrome. J Thorac Cardiovasc Surg. 1989;97(6):878-885.
29. Haggerty CM, de Zélicourt DA, Restrepo M, et al. Comparing pre- and post-operative Fontan hemodynamic simulations: implications for the reliability of surgical planning. Ann Biomed Eng. 2012;40(12):2639-2651.
30. Ceballos A, Argueta-Morales IR, Divo E, et al. Computational analysis of hybrid Norwood circulation with distal aortic arch obstruction and reverse Blalock-Taussig shunt. Ann Thorac Surg. 2012;94(5):1540-1550.
31. Smith Maia MM, Cortês TM, Parga JR, et al. Evolutional aspects of children and adolescents with surgically corrected aortic coarctation: clinical, echocardiographic, and magnetic resonance image analysis of 113 patients. J Thorac Cardiovasc Surg. 2004;127(3):712-720.
32. Lemler MS, Zellers TM, Harris KA, Ramaciotti C. Coarctation index: identification of recurrent coarctation in infants with hypoplastic left heart syndrome after the Norwood procedure. Am J Cardiol. 2000;86(6):697-699, A9.
33. Schievano S, Migliavacca F, Coats L, et al. Percutaneous pulmonary valve implantation based on rapid prototyping of right ventricular outflow tract and pulmonary trunk from MR data. Radiology. 2007;242(2):490-497.
34. Ibrahim D, Broilo TL, Heitz C, et al. Dimensional error of selective laser sintering, three-dimensional printing and PolyJet models in the reproduction of mandibular anatomy. J Craniomaxillofac Surg. 2009;37(3):167-173.
35. Idelchik IE. Handbook of Hydraulic Resistance, 2nd ed. New York, NY: Hemisphere Publishing; 1986
36. Quarteroni A, Veneziani A. Analysis of a geometrical multiscale model based on the coupling of PDE's and ODE's for blood flow simulations. Multiscale Model Simul. 2003;1(2): 173-195.
37. Varghese SS, Frankel SH, Fischer PF. Modeling transition to turbulence in eccentric stenotic flows. J Biomech Eng. 2008;130(1):014503.
38. http://www.dow.com/safechem/optim/optim-advantage/physical-properties.htm. Accessed April 24, 2014.
39. Lanzarone E, Vismara R, Fiore GB. A new pulsatile volumetric device with biomorphic valves for the *in vitro* study of the cardiovascular system. Artif Organs. 2009;33(12):1048-1062.
40. Januszewska K, Stebel A, Malec E. Consequences of right ventricle-to-pulmonary artery shunt at the first stage for the Fontan operation. Ann Thorac Surg. 2007;84(5):1611-1617.
41. Biglino G, Verschueren P, Zegels R, Taylor AM, Schievano S. Rapid prototyping compliant arterial phantoms for *in vitro* studies and device testing. J Cardiovasc Magn Reson. 2013; 15:2.
42. Goodwin JA, van Meurs WL, Sá Couto CD, Beneken JE, Graves SA. A model for educational simulation of infant cardiovascular physiology. Anesth Analg. 2004;99(6):1655-1664.